Oxygen-related traps in pentacene thin films: Energetic position and implications for transistor performance

Wolfgang L. Kalb,* Kurt Mattenberger, and Bertram Batlogg
Laboratory for Solid State Physics, ETH Zurich, 8093 Zurich, Switzerland
(Received 22 April 2008; revised manuscript received 29 June 2008; published 29 July 2008)

We studied the influence of oxygen on the electronic trap states in a pentacene thin film. This was done by carrying out gated four-terminal measurements on thin-film transistors as a function of temperature and without ever exposing the samples to ambient air. Photo-oxidation of pentacene is shown to lead to a peak of trap states centered at 0.28 eV from the mobility edge, with trap densities of the order of 10^{18} cm^{-3}. As the gate voltage is ramped up, these trap states are occupied at first and cause a reduction in the number of free carriers at a given gate voltage. Moreover, the exposure to oxygen reduces the mobility of the charge carriers above the mobility edge. We correlate the change of these transport parameters with the change of the essential device parameters, i.e., subthreshold performance and effective field-effect mobility. This study supports the assumption of a mobility edge for charge transport and contributes to a detailed understanding of an important degradation mechanism of organic field-effect transistors. Deep traps in an organic field-effect transistor reduce the effective field-effect mobility by reducing the number of free carriers and their mobility above the mobility edge.

DOI: 10.1103/PhysRevB.78.035334 PACS number(s): 73.20.Hb, 73.61.Ph, 73.20.At, 85.30.−z

I. INTRODUCTION

Organic semiconductors are among the most promising candidates for the future's flexible and low-cost electronics. Apart from the processability from solution or by thermal evaporation, a huge potential lies in tailoring the properties of the organic semiconductor by means of synthetic organic chemistry.

Charge carrier mobilities in organic field-effect transistors are comparable to the mobilities in hydrogenated amorphous silicon transistors and are adequate for many applications.[1,2] Critical issues, however, are electrical stability and environmental stability. The electrical stability of both *n*- and *p*-type organic semiconductor transistors has recently been shown to be very high if suitable gate dielectrics are used.[3,4] The environmental stability of the organic semiconductor, thus, is an urgent issue to be addressed.[5,6] Studies of the degradation of organic field-effect transistors are rare and indicate that in the case of *p*-type organic semiconductors, atmospheric oxygen or ozone is a major cause.[7–11] It is crucial to understand in detail the way in which an oxidation of the organic semiconductor impedes the charge transport and thus degrades the transistor characteristics.

The charge transport in crystalline organic semiconductors such as pentacene may be described by assuming a mobility edge, which separates extended and localized states. The charge carriers are transported in the extended states above the mobility edge, but are trapped by and thermally released from localized trap states below the mobility edge.[12–15] The mobility edge may be identified with the valence or conduction-band edge. However, the parameters dominating charge transport are the trap densities as a function of energy relative to the mobility edge, the number of delocalized charge carriers above the mobility edge, and the mobility of the latter charge. In highly disordered organic semiconductors, a description of the charge transport by variable range hopping may be more appropriate. Importantly, this situation can be described by trap-controlled transport in a transport level with a distribution of localized states below the transport level and is thus very similar to the mobility-edge picture.[16]

Organic field-effect transistors are excellent tools to study the charge transport in organic semiconductors since the position of the quasi-Fermi level at the dielectric-semiconductor interface can be fine-tuned by applying a gate voltage.[13,14,17–21]

Here we report on an extended study of pentacene thin-film transistors. Organic field-effect transistors were characterized by temperature-dependent measurements without ever exposing the samples to ambient air and after controlled exposure to oxygen and light. The effect of oxygen can only be clarified with pristine samples. Moreover, since the field-effect conductivity depends (approximately) exponentially on temperature, temperature is a very sensitive parameter.

Another distinct feature of our study is the gated four-terminal measurements instead of the commonly employed gated two-terminal measurements. This approach has previously been used to estimate basic parameters such as the effective field-effect mobility and the contact resistance.[22,23] The contact resistance can significantly affect the field-effect mobility. Consequently, contact effects may also lead to errors, e.g., in the trap densities as extracted from transistor characteristics.

In order to assess the fundamental transport parameters we have developed a scheme for organic field-effect transistors that is easy to use. The approach readily reveals all the key parameters with high accuracy in a straightforward and unambiguous fashion. The scheme is based on a method developed by Grünewald *et al.*[24] for amorphous silicon field-effect transistors. Instead of estimating the interface potential from the transistor characteristic measured at a single temperature as in the original scheme, we extract the interface potential from the temperature dependence of the field-effect conductivity.

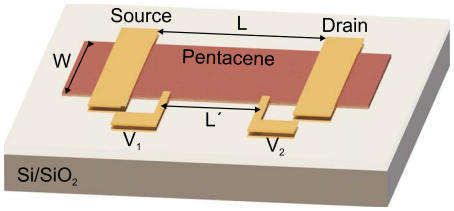

FIG. 1. (Color online) The transistors for the gated four-terminal measurements consisted of a well-defined stripe of pentacene with a width of $W=1000$ μm and gold electrodes. The distance between source and drain was $L=450$ μm. The voltage-sensing electrodes were used to measure the potentials V_1 and V_2 with respect to the grounded source and were separated by $L'=300$ μm.

II. EXPERIMENT

The system used in this study allows for the fabrication and characterization of organic thin-film transistors without breaking the high vacuum of order 10^{-8} mbar between the fabrication and measurement steps. It consists of a prober station connected to an evaporation chamber. The prober station contains a cryostat for temperature-dependent measurements. A schematic drawing of the system can be found in Ref. 25.

Heavily doped Si wafers with a 260-nm thick SiO_2 layer were cut, cleaned with hot solvents, fixed on a sample holder, and were then introduced into the cryo-pumped evaporation chamber of the device fabrication and characterization system. After approximately 24 h, two times sublimation purified pentacene was evaporated onto the samples through a shadow mask at a base pressure of the order of 10^{-8} mbar. The substrates were kept at room temperature during the evaporation and the final film thickness was 50 nm. The sample holder with the samples was then placed on a shadow mask for the gold evaporation without breaking the high vacuum, and gold electrodes were evaporated onto the pentacene. The completed thin-film transistors had a channel length of $L=450$ μm and a channel width of $W=1000$ μm. Moreover, two voltage-sensing electrodes were situated at $(1/6)L$ and $(5/6)L$ and had little overlap with the "masked" pentacene film, as schematically shown in Fig. 1. The alignment was achieved by means of a high-precision mask positioning mechanism. The sample holder was then transferred to and clamped on the cryostat in the turbo-pumped prober station of the device fabrication and characterization system without breaking the high vacuum (10^{-8} mbar).

A previous study revealed that the device performance improves with time when pentacene thin-film transistors are kept in high vacuum.[25] Therefore, the devices were kept in the prober station at a pressure of $\approx 2\times 10^{-8}$ mbar for approximately three weeks before starting the study. After that time, the device characteristics were found to be stable on the timescale of several days.

The prober station is equipped with five microprobers. The prober arms are connected to the cryostat with thick copper braids and are thus cooled when the cryostat and the sample holder with the samples are cooled down. For the temperature-dependent gated four-terminal measurements, the source, the drain, and the voltage-sensing electrodes were contacted with thin gold wires attached to four of the microprobers. By means of an electrical feedthrough to the cryostat, a gate bias could be applied. In order to measure the temperature on the surface of the samples, an AuFe/Chromel thermocouple was attached on the 5th microprober and was carefully pressed against the surface of the sample at each temperature.

The electrical measurements were carried out with an HP 4155A semiconductor parameter analyzer. Transfer characteristics were measured with a drain voltage of $V_d=-2$ V in steps of 0.2 V with an integration time of 20 ms and a delay time of 100 ms. For each gate voltage V_g, the drain current I_d and the potentials V_1 and V_2 between the grounded source electrode and the respective voltage sensing electrode were measured (Fig. 1). All electrical measurements were done in the dark.

The devices were exposed to oxygen by introducing 1 bar of oxygen (purity $\geq$99.9999 vol%) into the prober station through a leak valve. The pressure of the oxygen in the prober station was measured with a mechanical pressure gauge. In addition, the samples were also exposed to a combination of 1 bar of oxygen and white light from a cold light source (color temperature 3200 K).

III. CHARGE TRANSPORT PARAMETERS

Our approach consists of measuring the transfer characteristics at a low drain voltage ($V_d=-2$ V). This may be understood as staying as close as possible to the "unperturbed" situation, where charge is accumulated by a gate voltage in a metal-insulator-semiconductor (MIS) structure but no drain voltage is applied.[26] We begin by specifying the basic parameters to be extracted from the transfer characteristics.

A. Field-effect conductivity, field-effect mobility, and contact resistance

As described in Ref. 25 in more detail, the field-effect conductivity σ is given by

$$\sigma(V_g) = \frac{L}{W}\frac{I_d}{V_d}, \tag{1}$$

and is free from contact effects when calculated with

$$\sigma(V_g) = \frac{L'}{W}\frac{I_d}{(V_1 - V_2)}. \tag{2}$$

The field-effect mobility μ_{eff} in the linear regime is generally estimated with

$$\mu_{\text{eff}}(V_g) = \frac{L}{WV_dC_i}\left(\frac{\partial I_d}{\partial V_g}\right)_{V_d}. \tag{3}$$

This mobility is not influenced by the contact resistance if calculated with

$$\mu_{\text{eff}}(V_g) = \frac{L'}{W(V_1 - V_2)C_i}\left(\frac{\partial I_d}{\partial V_g}\right)_{V_d}. \tag{4}$$

We use the terms "two-terminal conductivity" and "four-terminal conductivity" for the expressions defined, respec-

tively, in Eqs. (1) and (2). Equation (3) is the "two-terminal mobility" and Eq. (4) is the "four-terminal mobility." μ_{eff}, as calculated with Eqs. (3) or (4), is an effective mobility. For a p-type semiconductor such as pentacene, it is a rough estimate of the ratio of the free surface hole density P_{free} to the total surface hole density P_{total} multiplied with the mobility μ_0 of the holes in the valence band, i.e.,

$$\mu_{\text{eff}} \approx \frac{P_{\text{free}}}{P_{\text{total}}}\mu_0. \tag{5}$$

Assuming a linear voltage drop all along the transistor channel, the total contact resistance can be approximated as

$$R_{\text{contact}}(V_g) = \frac{V_d - (V_1 - V_2)L/L'}{I_d} \tag{6}$$

and should be compared to the channel resistance of the device as given by

$$R_{\text{channel}}(V_g) = \frac{(V_1 - V_2)L/L'}{I_d}. \tag{7}$$

In order to gain a deeper insight into the physics of the organic semiconductor in a field-effect transistor, a more sophisticated description is developed in the following.

B. Spectral density of trap states and free hole density

The transistor characteristics critically depend on trap states. We treat the polycrystalline pentacene layer as uniform and assume that trap states on the surface of the gate dielectric only contribute to a nonzero flatband voltage. Consequently, the trap densities to be determined are an average over in-grain and grain boundary regions and may also be influenced, to some extent, by trap states on the surface of the gate dielectric.

In the following, we outline how a straightforward conversion of Poisson's equation, along with boundary conditions, eventually leads to the key equations. We assume that the electrical potential $V(x)$ at the surface of the pentacene film of thickness d vanishes under all biasing conditions, i.e.,

$$V(x = d) = 0. \tag{8}$$

The electric field F at this position is also assumed to drop to zero:

$$F = -\frac{d}{dx}V(x = d) = 0. \tag{9}$$

This is reasonable as long as the pentacene film is thicker than the decay length of the potential.[24] The situation is depicted in Fig. 2. The dielectric strength at the insulator-semiconductor interface must be continues, i.e., for a zero flatband voltage

$$\epsilon_i \frac{V_g - V_0}{l} = -\epsilon_s \frac{d}{dx}V(x = 0). \tag{10}$$

l is the thickness of the gate dielectric, ϵ_i and ϵ_s are the dielectric constants of the gate insulator and the semiconductor, and $V(x=0)=V_0$ is the interface potential. As detailed in

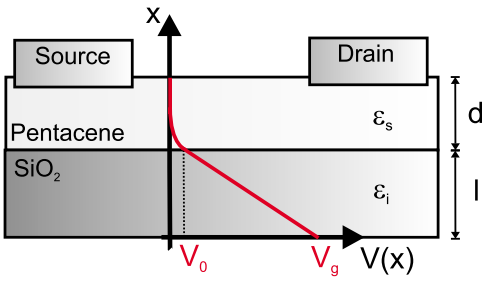

FIG. 2. (Color online) Potential drop across the gate insulator (thickness l, dielectric constant ϵ_i) and the pentacene thin film (thickness d, dielectric constant ϵ_s). Most of the gate voltage drops across the gate dielectric. At the insulator-semiconductor interface the potential is V_0.

Ref. 24, a conversion of Poisson's equation with these boundary conditions eventually leads to an expression for the total hole density p as a function of the interface potential V_0:

$$p(V_0) = \frac{\epsilon_0 \epsilon_i^2}{\epsilon_s l^2 e} U_g \left(\frac{dV_0}{dU_g}\right)^{-1}. \tag{11}$$

p (lower case) denotes a volume density of holes. The volume density depends on the distance x from the insulator-semiconductor interface, i.e., on the electrical potential $V(x)$ in the semiconductor. The volume density p and the surface hole density P are related by integrating over the depth of the whole film, i.e., $P=\int_0^d p(x)dx$. Equation (11) yields the functional dependence of the volume density of holes on the potential V_0. Moreover,

$$U_g = |V_g - V_{FB}| \tag{12}$$

in Eq. (11) is the gate voltage above the flatband voltage V_{FB}. Since the total hole density p can be written as

$$p(V) = \int_{-\infty}^{+\infty} N(E)[f(E - eV) - f(E)]dE, \tag{13}$$

its derivative is given by

$$\frac{1}{e}\frac{dp(V)}{dV} = \int_{-\infty}^{+\infty} N(E)\left|\frac{df(E - eV)}{d(E - eV)}\right| dE. \tag{14}$$

Equation (14) is a convolution of the density of states (DOS) function $N(E)$ with the derivative of the Fermi function. We approximate the Fermi function with a step function according to the common zero-temperature approximation.[13,25,27] Its derivative then is a delta function and we eventually have

$$\frac{1}{e}\frac{dp(V_0)}{dV_0} \approx N(E_F + eV_0). \tag{15}$$

From Eqs. (11) and (15) we can see that the interface potential V_0 as function of the gate voltage is the key to the DOS function. Since the change of the interface potential and the change of the drain current with gate voltage are linked, it is possible to extract the interface potential from the transfer characteristic measured at a single temperature.[24] Once the interface potential is known, the trap DOS in the mobility

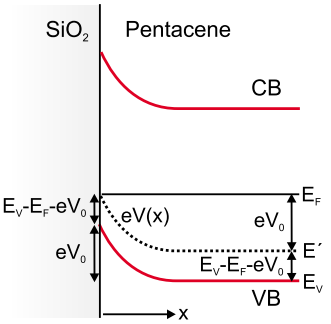

FIG. 3. (Color online) Gate-voltage-induced band bending at the insulator-semiconductor interface. At a given gate voltage, the band shift at the interface is eV_0. The energy of trap states with an energy E' is raised at the interface and now coincides with the Fermi energy E_F of the sample. The energy of these trap states relative to the energy of the mobility edge E_V is $E_V-E_F-eV_0$ and is approximated by the experimentally available activation energy E_a of the field-effect conductivity.

gap can be estimated with Eqs. (11) and (15). Thus, the trap densities can be plotted as a function of the band shift eV_0 at the interface, which is the energy of the traps relative to the Fermi energy of the sample (Fig. 3). In a previous study we have applied this method to four-terminal conductivity data.[25] For the present study we have advanced the extraction scheme. As described in the following, we used gated four-terminal measurements at various temperatures to estimate the interface potential. We then used Eqs. (11) and (15) to calculate the DOS. The consistency of the assumption of charge transport above a mobility edge with the temperature-dependent measurements provides a greater degree of confidence to any conclusion. Moreover, the latter approach has the advantage of eventually giving the DOS as a function of energy relative to the mobility edge.

We now show that the activation energy $E_a(V_g)$ of the field-effect conductivity as defined by

$$\sigma(V_g) = A \exp\left(-\frac{E_a}{kT}\right) \tag{16}$$

and as determined with Arrhenius plots is related to the band shift eV_0 at the insulator-semiconductor interface. Following Boltzmann's approximation, the field-effect conductivity

$$\sigma(V_g) = e\mu_0 P_{\text{free}} \tag{17}$$

may be written as

$$\sigma(V_g) = e\mu_0 \int_0^d p_{\text{free}} dx$$

$$= e\mu_0 N_V \exp\left(-\frac{E_V - E_F}{kT}\right) \times \int_0^d \exp\left(\frac{eV(x)}{kT}\right) dx. \tag{18}$$

N_V is the effective (volume) density of extended states, E_V is the energetic position of the mobility edge, and E_F is the Fermi energy. As an example we consider an exponential trap DOS

$$N(E) = N_0 \exp\left(\frac{E}{kT_0}\right) \tag{19}$$

with a characteristic slope of kT_0. If we assume that all the gate-induced charge is trapped, integration of the exponential trap DOS leads to a simple exponential dependence of the total hole density p on the potential $V(x)$, which is

$$p \propto \exp\left(\frac{eV}{kT_0}\right). \tag{20}$$

This approximation is not expected to lead to serious errors as long as the majority of the gate-induced charge is trapped.[28] With Eq. (20) it can be shown that, except for small values of V, also the electric field F perpendicular to the insulator-semiconductor interface exponentially depends on V as

$$F \propto \exp\left(\frac{eV}{2kT_0}\right). \tag{21}$$

Reference 13 shows in detail how the electric field as in Eq. (21) results in an expression for the free surface hole density P_{free} in Eq. (17). This expression is

$$P_{\text{free}} \approx \frac{2kT\epsilon_0\epsilon_s}{eC_iU_g} \frac{l}{2l-1} N_V \exp\left(-\frac{E_V - E_F}{kT}\right) \times \left[\exp\left(\frac{eV_0}{kT}\right) - \exp\left(\frac{eV_0}{2lkT}\right)\right], \tag{22}$$

where

$$l = \frac{T_0}{T}. \tag{23}$$

The second exponential term in Eq. (22) can safely be neglected and so we have

$$P_{\text{free}} \approx L_a \frac{l}{2l-1} N_V \exp\left(-\frac{E_V - E_F - eV_0}{kT}\right), \tag{24}$$

with

$$L_a = \frac{2kT\epsilon_0\epsilon_s}{eC_iU_g}. \tag{25}$$

The factor $l/(2l-1)$ is expected to be close to unity and L_a may be understood as the effective thickness of the accumulation layer.[29] Small deviations from an exponential trap DOS might be considered with a variable parameter l. However, the variation of l can be ignored when compared to the exponential term in Eq. (24). If we compare Eq. (24) with Eqs. (16) and (17), we eventually have

$$E_a \approx E_V - E_F - eV_0 = E_V - E_F'. \tag{26}$$

The measured activation energy of the field-effect conductivity $E_a(V_g)$ is approximately equal to the energetic difference between the Fermi level E_F and the mobility edge at the interface, as indicated in Fig. 3. E_F', as defined in Eq. (26), is the quasi-Fermi level at the insulator-semiconductor interface. By substituting $dV_0 = -dE_a/e$ in Eqs. (11) and (15), we finally have the DOS

$$N(E) \approx \frac{d}{dE_a}\left[\frac{\epsilon_0 \epsilon_i^2}{\epsilon_s l^2} U_g \left(\frac{dE_a}{dU_g}\right)^{-1}\right] \tag{27}$$

as a function of the energy $E=E_V-E_F' \approx E_a(V_g)$ relative to the mobility edge.

C. Fraction of free holes and band mobility

The fraction of free holes $P_{\text{free}}/P_{\text{total}}$ is of crucial importance since it is proportional to the effective field-effect mobility as described by Eq. (5). It can readily be extracted from temperature-dependent measurements. From Eqs. (24) and (26) and with the total surface hole density

$$P_{\text{total}} = C_i U_g / e, \tag{28}$$

we eventually have

$$\frac{P_{\text{free}}}{P_{\text{total}}} = \frac{L_a e}{C_i U_g} \frac{l}{2l-1} N_V \exp\left(-\frac{E_a}{kT}\right). \tag{29}$$

Finally, from Eq. (17) we see that the band mobility μ_0 can be estimated with

$$\mu_0 = \sigma/(eP_{\text{free}}). \tag{30}$$

IV. RESULTS

A. Extraction method and the influence of the contact resistance

In this section, we demonstrate the extraction of the DOS and the hole densities from a set of gated four-terminal measurements. Moreover, we analyze the influence of the contact resistance on these functions.

In a first step, we derived the activation energy $E_a(V_g)$ of the four-terminal conductivity as a function of the gate voltage, according to Eq. (16). Figure 4 shows Arrhenius plots and the corresponding linear regression lines. We found that only currents equal to or above ≈1 nA are usable in the sense that the corresponding four-terminal conductivity follows a straight line in an Arrhenius plot. Therefore, we used all currents above 1 nA for the extraction of the activation energy. At low gate voltages, only the measurements at the highest temperatures were considered as a consequence of the 1 nA limit. The final result is shown in Fig. 5. The activation energy $E_a(V_g)$ was then represented by a smooth fit (red/gray line in Fig. 5) in order to suppress the noise in the data.

Finally, the DOS was obtained with Eq. (27) and is plotted as a function of the energetic distance to the mobility edge $E_a(V_g) \approx E_V - E_F'$. For the calculations, the dielectric constant of pentacene was assumed to be $\epsilon_s=3$. In order to determine $U_g=|V_g-V_{FB}|$ in Eq. (27), the flatband voltage V_{FB} was assumed to be equal to the device onset voltage at room temperature. The onset voltage is the gate voltage where the drain current sharply rises when plotted on a logarithmic scale, i.e., where the drain current becomes measurable. The flatband voltage marks the onset of the accumulation regime, and a small difference between the flatband voltage and the onset voltage may thus exist. A scheme to extract the flatband voltage was developed for amorphous silicon-based transistors and this scheme involves the temperature dependence of the device off-current.[30] The scheme can, however, not be applied to our devices because the off-currents are due to experimental limitations and are not related to the conductivity of the pentacene thin film.

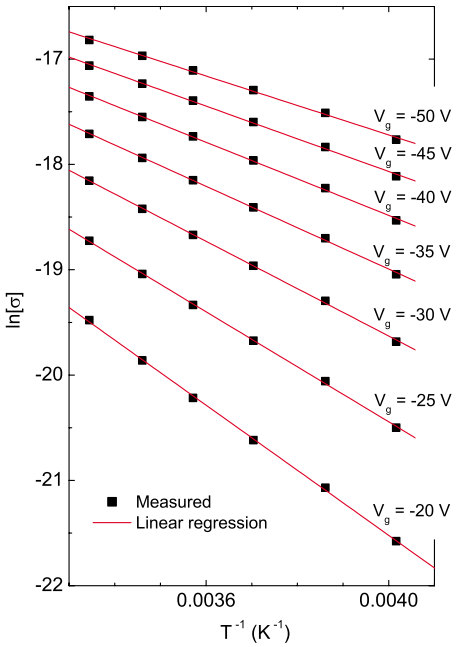

FIG. 4. (Color online) Arrhenius plots of the four-terminal conductivity at various gate voltages V_g. The activation energy $E_a(V_g)$ was derived from the slope of the linear regression lines.

Figure 6 (circles) shows the DOS as derived from the activation energy in Fig. 5. The procedure was also applied to the same data without correcting for the contact resistance, i.e., to the two-terminal conductivity. The dashed line in Fig. 6 is the result, highlighting the necessity to correct for the contacts. Even for long channel devices ($L=450$ μm), neglecting the contact resistance leads to significant errors in the shape and magnitude of the DOS, even more so closer to the mobility edge.

The free hole density, the total hole density, and the fraction of free holes were obtained with Eq. (24), Eq. (28) and

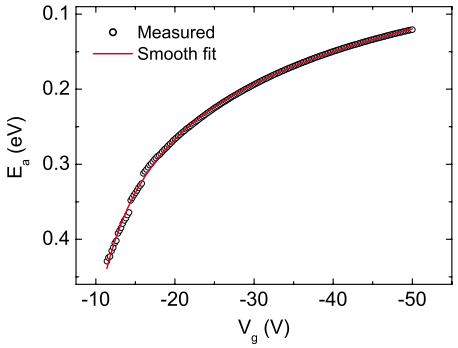

FIG. 5. (Color online) Activation energy $E_a(V_g)$ as determined with linear regressions according to Eq. (16) and as verified with Arrhenius plots (Fig. 4). The graph also shows a smooth fit of the activation energy (red/gray line).

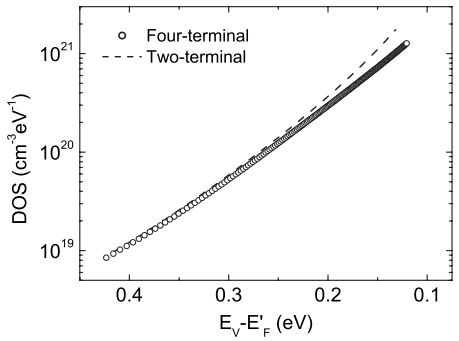

FIG. 6. Density of traps as a function of energy relative to the mobility edge (circles). The dashed line was extracted from the same set of temperature-dependent measurements, but the contact resistance was neglected. The contact resistance can lead to significant errors in the density of states function, particularly closer to the mobility edge.

Eq. (29), respectively. We have assumed that the effective density of extended states N_V is equal to the density of the pentacene molecules, i.e., $N_V=3\times10^{21}$ cm^{-3} and Fig. 7 is the result. For the given sample at high gate voltages, $\approx10\%$ of the holes that are induced by the gate are free, i.e., only this fraction actually contributes to the drain current.

B. Oxygen-related device degradation

This study correlates the oxygen-related degradation of the transistor characteristics with the change of the fundamental transport parameters. We begin by presenting the characteristic effects of oxygen on the pentacene transistor characteristics. The blue (gray) line in Fig. 8 is a transfer characteristic measured as grown (after a high-vacuum storage time of approximately three weeks). The sample was then exposed to 1 bar of oxygen for 19 h and, additionally, to 1 bar of oxygen and white light for 4 h. The red (gray) curve in Fig. 8 is a measurement of the same device after the oxidation process and after an evacuation time of 22 h at a base pressure of the order of 10^{-8} mbar. Figure 8 contains the forward and the reverse sweeps in both cases. Figure 9

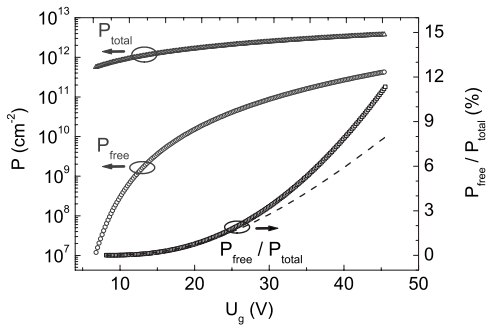

FIG. 7. Total hole density $P_{\text{total}}=C_iU_g/e$, free hole density P_{free} and fraction of free holes $P_{\text{free}}/P_{\text{total}}$ at room temperature as derived from the temperature dependence of the four-terminal conductivity. A significant fraction of the total gate-induced charge is trapped even at high gate voltages. The dashed line is the ratio $P_{\text{free}}/P_{\text{total}}$ if the contact resistance is neglected.

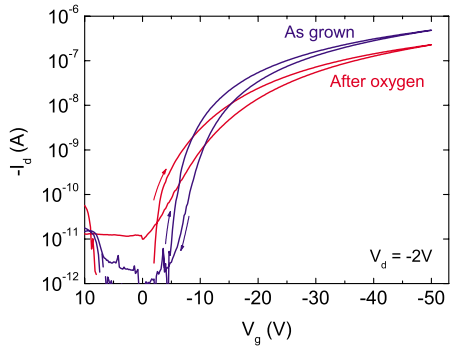

FIG. 8. (Color online) Linear regime transfer characteristic of a pentacene thin-film transistor measured as-grown (blue/gray line) and after oxidation (red/gray line). The graph shows the forward and the reverse sweeps in both cases. The characteristic oxygen-related degradation effects are a decrease in subthreshold performance, a decrease in on-current and a shift of the transfer characteristic to more positive voltages. The current hysteresis is essentially unaffected.

shows the corresponding four-terminal mobilities and, for comparison, the respective two-terminal mobilities. The degradation effects are the following: a significant degradation of the subthreshold performance, a decrease in on-current, a decrease in effective mobility, and a shift of the transfer characteristic toward more positive voltages. Also the contact resistance is increased after the oxygen exposure. At room temperature and $V_g=-50$ V it increases from the as-grown value of $R_{\text{contact}}W=2.8\times10^4$ Ω cm to 9.2×10^4 Ω cm after the oxygen exposure, i.e., it increases by a factor of 3.3. The increase in contact resistance may be due to the fact that the contact resistance is dominated by the film resistance. In a top-contact device, the holes must pass from the electrodes through the pentacene film to the channel at the insulator-semiconductor interface.[25,31] Importantly, before and after the oxygen exposure we have a device that is not limited by the contact resistance. At $V_g=-50$ V for example, the contact resistance R_{contact} is ≈14 times smaller than the channel resistance R_{channel} prior to the oxygen exposure and ≈9 times

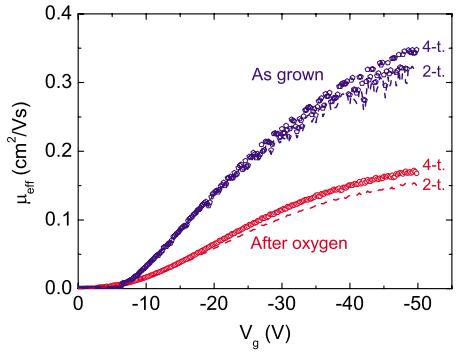

FIG. 9. (Color online) Four-terminal effective mobility (4-t) from an as-grown sample (blue/gray pentagons) and after the oxygen exposure (red/gray circles). At $V_g=-50$ V for example, the contact-corrected field-effect mobility decreases from $\mu_{\text{eff}}=0.35$ cm^2/Vs to 0.17 cm^2/Vs, i.e., it is reduced by a factor of 2.1. The dashed lines represent the respective two-terminal mobility (2-t) where the contact resistance is neglected.

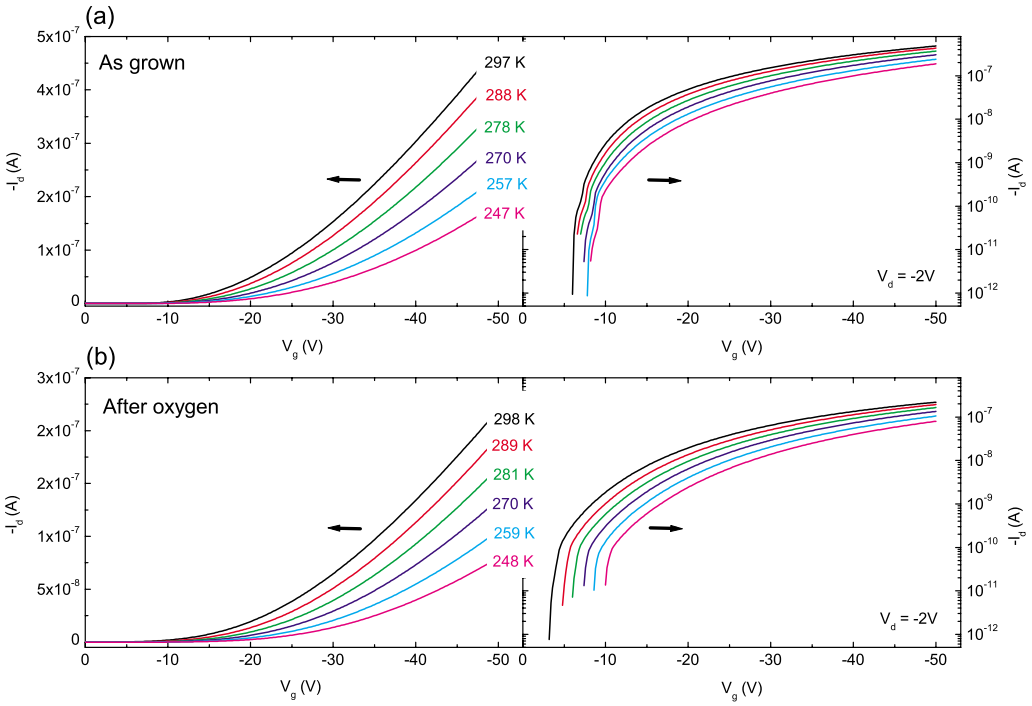

FIG. 10. (Color online) (a) Linear regime transfer characteristics at various temperatures from an as-grown sample, i.e., prior to oxygen exposure. (b) Transfer characteristics at similar temperatures after exposing the sample to 1 bar of oxygen for 23 h (19 h in the dark and 4 h in white light). The temperature dependence of the drain current in the subthreshold regime is much more pronounced after the oxygen exposure.

smaller than the channel resistance after the oxygen exposure.

The degradation effects can be observed when the transistor is subjected to oxygen in the dark. It is, however, much accelerated when the oxygen exposure is carried out in the presence of light, i.e., in the presence of activated oxygen and oxygen radicals.

The degradation of the subthreshold performance and the field-effect mobility is due to oxygen-related defects that cause electrically active trap states within the mobility gap. The shift of the transfer characteristic is due to a change of the flatband voltage. It is known that oxygen can cause changes of the flatband voltage in an organic semiconductor device.[32,33]

C. Oxygen-related traps

We now turn to the determination of the trap densities prior to and after the oxygen exposure. For the temperature-dependent gated four-terminal measurements, we used a low cooling rate (0.2–0.25°/min) in order not to damage the sample. In Fig. 10 we show the temperature dependence of the transfer characteristics prior to and after the oxygen exposure. The temperature-dependent measurements in Fig. 10 are from the same sample as the measurements in Figs. 8 and 9 and were carried out shortly after these measurements. The main difference after the oxygen exposure is that the temperature dependence in the subthreshold regime (drain currents on a logarithmic scale) is much more pronounced.

The DOS was extracted for both sets of measurements as described in Secs. III B and IV A. The main panel of Fig. 11 shows the final result on a logarithmic scale. The difference between two adjacent data points in Fig. 11 corresponds to a change of 0.2 V in the gate voltage. Some gate voltages U_g are indicated in the graph. The spacing between the data points decreases as the gate voltage is increased since at high gate voltages, it is increasingly difficult to shift the quasi-Fermi level E_F' toward the mobility edge due to the increased trap density.

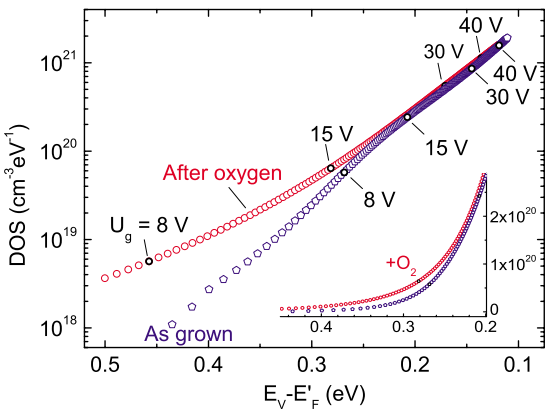

FIG. 11. (Color online) Main panel: DOS as a function of energy relative to the mobility edge on a logarithmic scale. The blue (gray) pentagons are trap densities measured prior to the oxygen exposure and the red (gray) circles are trap densities measured after the oxygen process. The oxidation of the pentacene film leads to a significant increase in traps that are somewhat deeper in energy. The corresponding gate voltage U_g above flatband is indicated. The inset shows the deeper traps on a linear scale.

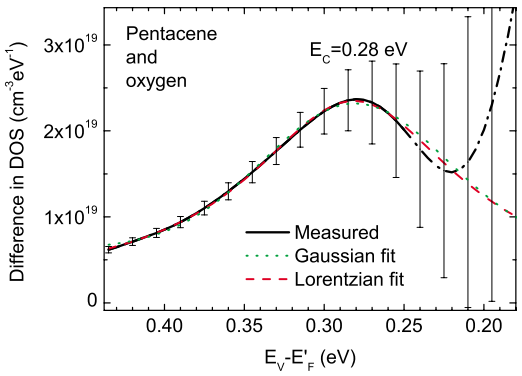

FIG. 12. (Color online) Difference of the DOS prior to and after the oxygen exposure (black line). A relative error of 5% is assumed for the determination of a trap DOS and this is indicated by the error bars. The oxygen exposure leads to a broad peak of trap states. A Gaussian fit for energies ≥ 0.25 eV (dotted green/gray line) gives good agreement with the measured curve and so does a Lorentzian fit (dashed red/gray line). The peak is centered at $E_C=0.28$ eV and the width and height of the peak are, respectively, 0.16 eV and 2.2×10^{19} cm^{-3} eV^{-1}. At energies ≤ 0.25 eV the difference in the DOS is comparable to or smaller than the estimated error and the DOS is essentially unaffected by the oxygen exposure.

We keep in mind that even in an ideal (trap-free) MIS structure, the interface potential increases with gate voltage more rapidly at low gate voltages than at high gate voltages. This is a screening effect. The screening depends on the total charge in the device and it increases with gate voltage.

The oxygen exposure leads to a significant increase in the density of traps that are somewhat deeper in energy (Fig. 11). The inset in Fig. 11 shows the deeper traps on a linear scale. In Fig. 12 we show the difference of the trap densities prior to and after the oxygen exposure on a linear scale (black line). We assume that our method allows for a determination of the DOS to an accuracy of 5% and this is indicated by the error bars in Fig. 12. At energies ≤ 0.25 eV from the mobility edge the difference in the DOS is comparable to or smaller than the estimated error and so for energies ≤ 0.25 eV, the DOS is essentially unaffected by the oxygen exposure. At larger energies, however, the oxygen exposure leads to a broad peak of trap states. The dotted green (gray) line in Fig. 12 is a Gaussian fit of the experimental data for energies ≥ 0.25 eV, and the dashed red (gray) line is a Lorentzian fit. In both cases good agreement is achieved. The Lorentzian fitting function is centered at $E_C=0.28$ eV and has a width of 0.16 eV and a height of 2.2×10^{19} cm^{-3} eV^{-1}. The area under the peak gives a volume trap density of $\approx 4\times10^{18}$ cm^{-3}. With a density of the pentacene molecules of 3×10^{21} cm^{-3}, this gives an oxygen-related impurity concentration of $\approx 0.1\%$ provided that each impurity results in one trap.

The DOS close to the mobility edge is well described by a single exponential function. A fit for energies ≤ 0.22 eV gives essentially identical characteristic slopes prior to and after the oxygen exposure, i.e., respectively, $kT_0=47$ meV and $kT_0=48$ meV. These values are in good agreement with characteristic slopes from pentacene-based field-effect transistors in the literature. A characteristic slope of $kT_0=40$ meV is reported as determined by simulating the measured transfer characteristics of pentacene thin-film transistors.[34] Characteristic slopes of $kT_0=32-37$ meV were derived from pentacene thin-film transistors with another device simulation program.[14,35] Yet another program gives a slope of $kT_0=100$ meV for pentacene thin-film transistors.[36] However, the band mobility μ_0 needs to be fixed for the simulations and depending on the choice of the band mobility, slopes of up to 400 meV are also used in Ref. 36. With the initial scheme by Grünewald *et al.*[25] and from similar pentacene thin-film transistors as in the present study we have extracted characteristic slopes of $kT_0=32$ meV shortly after the evaporation of the pentacene and of $kT_0=37$ meV in the aged thin film with reduced trap density. For a pentacene single-crystal device, a characteristic slope of $kT_0=109$ meV is reported.[18]

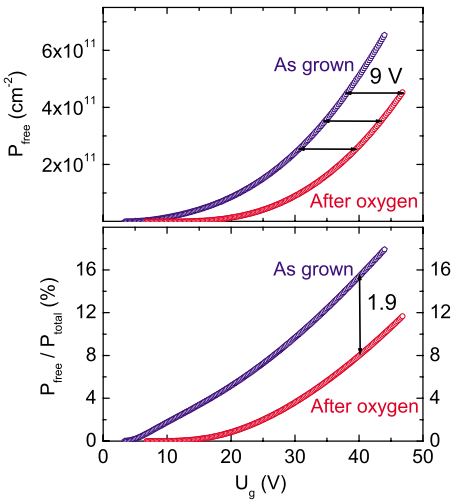

FIG. 13. (Color online) Upper panel: free hole density P_{free} prior to and after the oxygen exposure as derived from the temperature-dependent gated four-terminal measurements. After the oxygen exposure the curve is shifted by 9 V. The magnitude of the shift is closely linked to density of the additional traps. Additional trapped holes with a density of 5×10^{18} cm^{-3} can be estimated from the shift, which is highly consistent with the trap density estimated from an integration of the peak in Fig. 12 (4×10^{18} cm^{-3}). Lower panel: corresponding fraction of free holes functions $P_{\text{free}}/P_{\text{total}}$ prior to and after the oxygen exposure. At a given gate voltage U_g, the fraction of free holes is significantly reduced after the oxygen exposure. At $U_g=40$ V for example, the fraction of free holes drops from 15% to 8%, i.e., it is reduced by a factor of 1.9.

D. Trap-induced changes in the free hole density

The upper panel in Fig. 13 shows the free surface hole density [Eq. (24)] prior to and after the oxygen exposure from the two sets of temperature-dependent measurements in Fig. 10. The parameter $l=T_0/T$ was calculated with the characteristic slopes mentioned above: for room temperature $l=1.9$ $[l/(2l-1)=0.68]$ prior to and after the oxygen exposure. At sufficiently high gate voltages, the free hole density as a function of gate voltage is shifted by 9 V toward higher gate voltages as a consequence of the oxygen exposure.

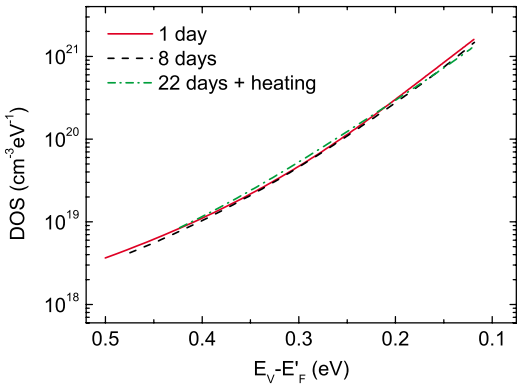

FIG. 14. (Color online) Trap densities after oxygen exposure. The re-evacuation time after the oxygen exposure is one day (full red/gray line), eight days (dashed black line) and 22 days (dash-dotted green/gray line). The oxygen-related traps are very stable, i.e., the DOS functions coincide. Prior to the last characterization after 22 days, the sample was slowly heated to temperatures up to 70 °C.

The corresponding fractions of the free holes $P_{\text{free}}/P_{\text{total}}$ were extracted according to Eq. (29) and are shown in the lower panel of Fig. 13. The fraction of the free holes changes significantly due to the oxygen exposure. At U_g=40 V for example, 15% of all the induced holes are free prior to the oxygen exposure and this fraction drops to 8% after the oxygen exposure. It is reduced by a factor of 1.9. A fraction of free holes of 8%–15% at 40 V is in good agreement with values for pentacene thin-film transistors found in the literature. In Ref. 35, a fraction of free holes around 10% is specified for comparable total gate-induced charge densities.

E. Stability of the oxygen-related defects

The DOS after the oxygen exposure was measured after a re-evacuation time of $\approx 22h$. In order to elucidate the stability of the oxygen-related traps, the sample was kept in the prober station at 10^{-8} mbar for an additional seven days period. After that time, temperature-dependent gated four-terminal measurements were carried out and the DOS was extracted. After these measurements, the sample was kept at 10^{-8} mbar for another ten days. The pentacene films were then slowly heated to 50 °C at a rate of 0.2°/min with an electrical heating element at the cryostat. The temperature was held for 2 h and the sample was then left to cool down. The same procedure was repeated with a final temperature of 70 °C. Due to the low heating and even lower cooling rates, the whole process took three days and the effective heating time was very long. Figure 14 shows the DOS after a re-evacuation time of ≈1 day (same as in Fig. 11), 8 days, and 22 days, the latter time including the heating procedure. The DOS functions are very similar and we can conclude that the oxygen-related trap states are very stable.

V. DISCUSSION

A. Effect of oxygen on the trap DOS

The DOS as extracted from the measurements of the as-grown sample is of particular interest since the sample was kept at a pressure of the order of 10^{-8} mbar all along. The trap densities are relatively high (10^{18}–10^{21} cm^{-3} eV^{-1}) with a rather smooth dependence on energy. In the case of the measurements on the as-grown samples, the effect of ambient gases can be excluded. It should be kept in mind that we used pentacene powder that was recrystallized twice in high vacuum. We conclude that the "amorphouslike" trap DOS measured with an as-grown sample is mainly due to structural defects within the pentacene. Trap states on the surface of the gate dielectric, caused by certain chemical groups for example, may also contribute to the states that are deeper in energy.

When pentacene is exposed to oxygen, the gas migrates into the pentacene film and interacts with the pentacene molecules. This effect is expected to be accelerated if, in the presence of light, oxygen is activated and its dissociation is aided. We observe significant and irreversible changes in the transfer characteristics and in the DOS caused by the oxygen exposure. It should be kept in mind, however, that several hours of exposure to 1 bar of oxygen are necessary in order to observe these changes. Consequently, pentacene thin-films are not very sensitive toward oxidation.

The oxygen exposure leads to a broad peak of trap states centered at 0.28 eV, as shown in Fig. 12. This suggests the degradation mechanism to be dominated by the creation of a specific oxygen-related defect. The large width of the peak (0.16 eV) is thought to result from local structural disorder that modifies the on-site energy of the oxygen-affected molecules. As a matter of fact, very similar arguments are used to explain the smooth distribution of trap states in hydrogenated amorphous silicon. Even small deviations in the local structure of a defect lead to a different electronic state.[37]

Theoretical studies predict various types of oxygen-related defects in pentacene.[38,39] In Ref. 38 oxygen defects are discussed in which a H atom of a pentacene molecule is replaced by an oxygen atom to form a $C_{22}H_{13}O$ molecule. The oxygen forms a double bond with the respective C atom, and the p_z orbital at this atom no longer participates in the π-electron system of the pentacene molecule. The oxidation at the middle ring is shown to be energetically most favorable. These oxygen defects are expected to lead to trap states in the mobility gap.[38] In Ref. 39 other oxygen defects are described. An example is a single oxygen intermolecular bridge, where a single oxygen atom is covalently bound to the carbon atoms on the center rings of two neighboring pentacene molecules. This defect, for instance, is calculated to lead to electrically active traps at 0.33 and 0.4 eV above the valence band maximum.[39]

B. Influence of oxygen-related traps on the field-effect mobility

It is immediately plausible that the oxygen-related traps, which are somewhat deeper in energy, lead to a degradation of the subthreshold performance of the thin-film transistors. We do, however, also observe a significantly decreased field-effect mobility after oxygen exposure. This can be understood as follows. The deep traps that are created by the oxi-

dation need to be filled at first, and the position of the quasi-Fermi level lags behind the position of the quasi-Fermi level before the oxygen exposure. This is indicated in Fig. 11 by labeling the corresponding gate voltages U_g. At the same gate voltage (which is proportional to the total gate-induced hole density), the quasi-Fermi level is further away from the mobility edge. The fraction of free holes, however, depends exponentially on the position of the quasi-Fermi level [Eq. (29)]. The field-effect mobility as described by Eq. (5) is proportional to $P_{\text{free}}/P_{\text{total}}$ and so a reduction in the fraction of free holes readily affects the field-effect mobility. At $U_g = 40$ V, for example, the fraction of free holes is reduced by a factor of 1.9 after the oxygen exposure (lower panel of Fig. 13).

In addition, it is quite possible that the mobility μ_0 of the delocalized charge above the mobility edge is changed after the oxygen exposure. With Eq. (30), this mobility is estimated to be $\mu_0 = 1.2$ cm^2/Vs prior to the oxygen exposure and $\mu_0 = 0.95$ cm^2/Vs after the oxygen exposure. We have a reduction by a factor of 1.3 and a change of the "intrinsic" charge transport. Conclusively, the major cause for the reduction of the effective field-effect mobility is occupancy statistics, and a reduction of the mobility above the mobility edge also plays a role.

The reduction in the mobility μ_0 might be explained by a scattering of charge carriers at the oxygen-related defects. Another indication that scattering plays an important role in organic field-effect transistors is the fact that the mobilities μ_0 that we extract are lower than the best field-effect mobilities (up to 5 cm^2/Vs) from pentacene thin-film transistors.[40] In addition, repeated purification of pentacene has been shown to lead to very high mobilities in pentacene single crystals.[41] This effect is attributed to reducing the concentration of the oxidized pentacene species 6,13-pentacenequinone, which degrades the transport properties by scattering the charge carriers.[41]

C. Consistency check: Trapped holes vs traps

The upper panel in Fig. 13 shows that the oxidation causes a shift of the curve for the free hole density P_{free} by $\Delta U_g = 9$ V. The same free hole density P_{free} is realized for different total hole densities P_{total}. Clearly, for an identical number of free holes the difference in the number of total holes must be attributed to a difference in the number of the trapped holes. Consequently, due to the oxygen-related traps we have additional holes that are trapped with a density of $C_i \Delta U_g / e = 7.5 \times 10^{11}$ cm^{-2}. Except at very low gate voltages above the flatband voltage, the charge in an organic field-effect transistor is concentrated at the insulator-semiconductor interface. As explained above, our extraction scheme only considers currents above 1 nA. Therefore it is reasonable to assume that the holes are trapped in a region at the insulator-semiconductor interface with a thickness of the order of one molecular layer (≈ 1.5 nm for pentacene). This gives a volume density of trapped holes of $\approx 5 \times 10^{18}$ cm^{-3}. By integrating the peak in the trap DOS we have derived a trap density of $\approx 4 \times 10^{18}$ cm^{-3}, which is in very good agreement with the density of the trapped holes.

D. Deep traps and device performance

This study reveals how an increase in the density of deeper traps can significantly affect the field-effect mobility. The influence of deep traps on the device characteristics is of most general concern because deep traps can have various origins. Trap states due to the surface of the gate dielectric, for example, are expected to be electronically deep traps. Modifying the gate dielectric with a self-assembled monolayer or using a polymeric gate dielectric not only leads to an improved subthreshold swing but can also result in improved mobility.[2,42] This also holds in the case of organic single-crystal transistors where the semiconductor is grown separately and growth-related effects can be excluded.[3,43,44] In the light of the present study, it seems possible that these effects can be solely understood with transport in extended states above a mobility edge and a distribution of trap states: a reduced number of deep traps leads to an increased number of free carriers above the mobility edge and to a higher mobility of that charge.

VI. SUMMARY AND CONCLUSIONS

Pentacene-based thin film transistors were characterized without exposing the samples to ambient air (as-grown) and after exposure to oxygen in combination with white light. The exposure of the pentacene to the oxidizing agent leads to a degradation of the subthreshold performance, a decrease in field-effect mobility, a shift of the flatband voltage, and an increased contact resistance.

Contact-corrected trap state functions were extracted from temperature-dependent gated four-terminal measurements. We show that the exposure to oxygen leads to a broad peak of trap states centered at 0.28 eV, with a width of 0.16 eV and a height of the order of 10^{19} cm^{-3} eV^{-1}. The emergence of a peak indicates the process to be dominated by the creation of a specific oxygen-related defect. The large width of the peak is due to the energetically different surroundings induced by structural disorder. The oxygen defects are very stable and are likely to be caused by pentacene molecules with covalently bound oxygen.

The decrease in field-effect mobility is caused by the oxygen-related deep traps. These states are filled upon increasing the gate voltage and the quasi-Fermi level at the interface lags behind the position it has in as-deposited samples. This leads to a significantly smaller fraction of free holes. The magnitude of the shift in the free hole function is highly consistent with the density of the oxygen-related traps ($\approx 4 \times 10^{18}$ cm^{-3}) as estimated from the difference in the trap DOS prior to and after the oxygen exposure. In addition, the oxygen exposure leads to a decrease in the mobility of the charge carriers above the mobility edge. This latter effect may be due to scattering of the charge carriers at the oxygen defects.

The results can be seen from a more general point of view. At first, the temperature-dependent measurements are self-consistent with the assumption of a mobility edge, thus contributing to an understanding of charge transport in organic semiconductors. Moreover, they are an example for the

way in which deeper traps can influence the effective field-effect mobility.

Theoretical studies may help to identify the oxygen defect, and organic synthetic chemistry may soon find a way to tailor organic semiconductors where the creation of defects by oxidation is completely inhibited.

ACKNOWLEDGMENTS

The authors thank Kurt Pernstich, David Gundlach, and Simon Haas for support in the early stages of the study and Thomas Mathis and Matthias Walser for stimulating discussions.

*kalb@phys.ethz.ch

[1] D. J. Gundlach *et al.*, Nat. Mater. **7**, 216 (2008).
[2] Y.-Y. Lin, D. J. Gundlach, S. F. Nelson, and T. N. Jackson, IEEE Trans. Electron Devices **44**, 1325 (1997).
[3] W. L. Kalb, T. Mathis, S. Haas, A. F. Stassen, and B. Batlogg, Appl. Phys. Lett. **90**, 092104 (2007).
[4] X.-H. Zhang, B. Domercq, and B. Kippelen, Appl. Phys. Lett. **91**, 092114 (2007).
[5] D. M. de Leeuw, M. M. J. Simenon, A. R. Brown, and R. E. F. Einerhand, Synth. Met. **87**, 53 (1997).
[6] T. D. Anthopoulos, G. C. Anyfantis, G. C. Papavassiliou, and D. M. de Leeuw, Appl. Phys. Lett. **90**, 122105 (2007).
[7] C. Pannemann, T. Diekmann, and U. Hilleringmann, J. Mater. Res. **19**, 1999 (2004).
[8] A. Maliakal, K. Raghavachari, H. Katz, E. Chandross, and T. Siegrist, Chem. Mater. **16**, 4980 (2004).
[9] F. De Angelis, S. Cipolloni, L. Mariucci, and G. Fortunato, Appl. Phys. Lett. **88**, 193508 (2006).
[10] M. L. Chabinyc, R. A. Street, and J. E. Northrup, Appl. Phys. Lett. **90**, 123508 (2007).
[11] H. Klauk, U. Zschieschang, R. T. Weitz, H. Meng, F. Sun, G. Nunes, D. E. Keys, C. R. Fincher, and Z. Xiang, Adv. Mater. (Weinheim, Ger.) **19**, 3882 (2007).
[12] P. W. Anderson, Proc. Natl. Acad. Sci. U.S.A. **69**, 1097 (1972).
[13] G. Horowitz, R. Hajlaoui, and P. Delannoy, J. Phys. III **5**, 355 (1995).
[14] K. P. Pernstich, B. Rössner, and B. Batlogg, Nat. Mater. **7**, 321 (2008).
[15] W. Warta and N. Karl, Phys. Rev. B **32**, 1172 (1985).
[16] V. I. Arkhipov, P. Heremans, E. V. Emelianova, G. J. Adriaenssens, and H. Bässler, Appl. Phys. Lett. **82**, 3245 (2003).
[17] F. Schauer, J. Appl. Phys. **86**, 524 (1999).
[18] D. V. Lang, X. Chi, T. Siegrist, A. M. Sergent, and A. P. Ramirez, Phys. Rev. Lett. **93**, 086802 (2004).
[19] A. Salleo, T. W. Chen, A. R. Völkel, Y. Wu, P. Liu, B. S. Ong, and R. A. Street, Phys. Rev. B **70**, 115311 (2004).
[20] M. F. Calhoun, C. Hsieh, and V. Podzorov, Phys. Rev. Lett. **98**, 096402 (2007).
[21] N. Kawasaki, T. Nagano, Y. Kubozono, Y. Sako, Y. Morimoto, Y. Takaguchi, A. Fujiwara, C. C. Chu, and T. Imae, Appl. Phys. Lett. **91**, 243515 (2007).
[22] J. Takeya, C. Goldmann, S. Haas, K. P. Pernstich, B. Ketterer, and B. Batlogg, J. Appl. Phys. **94**, 5800 (2003).
[23] P. V. Pesavento, R. J. Chesterfield, C. R. Newman, and C. D. Frisbie, J. Appl. Phys. **96**, 7312 (2004).
[24] M. Grünewald, P. Thomas, and D. Würtz, Phys. Status Solidi B **100**, K139 (1980).
[25] W. L. Kalb, F. Meier, K. Mattenberger, and B. Batlogg, Phys. Rev. B **76**, 184112 (2007).
[26] G. Horowitz, P. Lang, M. Mottaghi, and H. Aubin, Adv. Funct. Mater. **14**, 1069 (2004).
[27] D. Braga, N. Battaglini, A. Yassar, G. Horowitz, M. Campione, A. Sassella, and A. Borghesi, Phys. Rev. B **77**, 115205 (2008).
[28] W. E. Spear and P. G. Le Comber, J. Non-Cryst. Solids **8-10**, 727 (1972).
[29] G. Horowitz, M. E. Hajlaoui, and R. Hajlaoui, J. Appl. Phys. **87**, 4456 (2000).
[30] R. L. Weisfield and D. A. Anderson, Philos. Mag. B **44**, 83 (1981).
[31] P. V. Pesavento, K. P. Puntambekar, C. D. Frisbie, J. C. McKeen, and P. P. Ruden, J. Appl. Phys. **99**, 094504 (2006).
[32] E. J. Meijer, A. V. G. Mangnus, B.-H. Huisman, G. W. 't Hooft, D. M. de Leeuw, and T. M. Klapwijk, Synth. Met. **142**, 53 (2004).
[33] A. Wang, I. Kymissis, V. Bulovic, and A. I. Akinwande, Appl. Phys. Lett. **89**, 112109 (2006).
[34] A. R. Völkel, R. A. Street, and D. Knipp, Phys. Rev. B **66**, 195336 (2002).
[35] D. Oberhoff, K. P. Pernstich, D. J. Gundlach, and B. Batlogg, IEEE Trans. Electron Devices **54**, 17 (2007).
[36] S. Scheinert, K. P. Pernstich, B. Batlogg, and G. Paasch, J. Appl. Phys. **102**, 104503 (2007).
[37] R. A. Street, *Hydrogenated Amorphous Silicon* (Cambridge University Press, Cambridge, England, 1991).
[38] J. E. Northrup and M. L. Chabinyc, Phys. Rev. B **68**, 041202(R) (2003).
[39] L. Tsetseris and S. T. Pantelides, Phys. Rev. B **75**, 153202 (2007).
[40] T. W. Kelley, D. V. Muyres, P. F. Baude, T. P. Smith, and T. D. Jones, *Organic and polymeric materials and devices*, MRS Symposia Proceedings Vol. 771 (Materials Research Society, Pittsburgh, 2003), p. L6.5.1.
[41] O. D. Jurchescu, J. Baas, and T. T. M. Palstra, Appl. Phys. Lett. **84**, 3061 (2004).
[42] J. Veres, S. Ogier, G. Lloyd, and D. de Leeuw, Chem. Mater. **16**, 4543 (2004).
[43] V. Podzorov, S. E. Sysoev, E. Loginova, V. M. Pudalov, and M. E. Gershenson, Appl. Phys. Lett. **83**, 3504 (2003).
[44] C. Goldmann, C. Krellner, K. P. Pernstich, S. Haas, D. J. Gundlach, and B. Batlogg, J. Appl. Phys. **99**, 034507 (2006).